Towards Flexible Sheet Cameras: Deformable Lens Arrays with Intrinsic Optical Adaptation

Daniel C. Sims   Yonghao Yue   Shree K. Nayar

Department of Computer Science, Columbia University
New York, NY 10027, USA

dcs2140@columbia.edu

Abstract

We propose a framework for developing a new class of imaging systems that are thin and flexible. Such an imaging sheet can be flexed at will and wrapped around everyday objects to capture unconventional fields of view. Our approach is to use a lens array attached to a sheet with a 2D grid of pixels. A major challenge with this type of a system is that its sampling of the scene varies with the curvature of the sheet. To avoid undesirable aliasing effects due to under-sampling in high curvature regions of the sheet, we design a deformable lens array with adaptive optical properties. We show that the material and geometric properties of the lens array can be optimized so that the object-side point spread function corresponding to each pixel widens with the curvature of the sheet at that pixel. This intrinsic adaptation of focal length is passive (without the use of actuators or other control mechanisms), and enables a sheet camera to capture images without aliasing, irrespective of its shape. We have designed a 33x33 lens array, fabricated it using silicone rubber, and conducted several experiments to verify its optical adaptation characteristics. We conclude with a discussion on the advantages of our proposed approach as well as future work.

1. Introduction

In the past decade, we have witnessed the miniaturization of the camera. This trend has been driven in great part by the explosive growth of the smartphone market. The desire of manufacturers to provide customers with thinner and cheaper camera phones has dramatically driven down the size and cost of imaging modules. Today, one can find image sensors in the market with pixels that are close to 1 micron in size. We have also seen imaging lenses become more compact while maintaining high performance. Owing to these developments, it is possible today to capture high resolution images from a single viewpoint using a compact and inexpensive device.

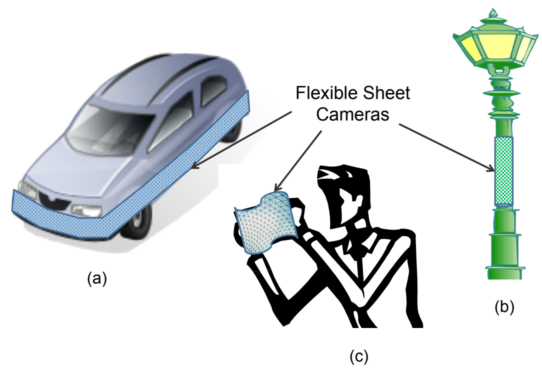

Figure 1. Examples of applications of flexible sheet cameras.

In this paper, we pursue a radically different approach to imaging. Rather than seeking to capture the world from a single point in space, our goal is to explore the idea of imaging using a thin, large, flexible sheet. If such cameras can be made at a low cost (ideally, like a roll of plastic sheet), they can be used to image the world in ways that would be difficult to achieve using one or more conventional cameras. In the most general sense, such an imaging system would enable any surface in the real world to capture visual information [9]. While there is significant ongoing work on the development of flexible image sensors [7, 9], our interest here is in the design of the optics needed to form images on such sensors.

In Figure 1(a), the sheet has been wrapped around a vehicle such that it captures a contiguous image of its surrounding. In the context of autonomous vehicles, such a system would provide situational awareness without blind-spots. Figure 1(b) shows how a sheet camera can be wrapped around a common urban artifact such as a lamp pole to provide 360 degree video of a public space.

Figure 1(c) shows how a flexible sheet camera can be

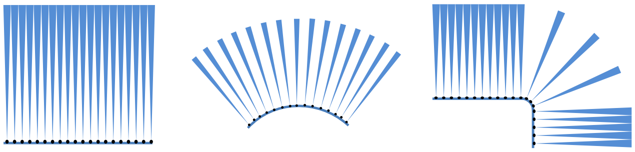

Figure 2. A fundamental problem with any flexible sheet camera is that scene sampling depends on the shape of the sheet. With a conventional (fixed focal length) lens array, this results in aliasing in regions of high sheet curvature. While the scene is adequately sampled in (a) where the sheet is flat, it is undersampled in (b) where the sheet is curved and (c) where the sheet is severely bent.

used in the context of photography. In this case, one side of the sheet is an imaging system while the other side is a display that directly shows what is being imaged. In addition to being thin and easy to carry around (like a credit card), the field of view of the camera can be adjusted by simply flexing the sheet. One can imagine several other uses of sheet cameras. For instance, they can be attached (like paper) to everyday surfaces such as walls and tabletops. In the case of a tabletop, the camera can provide information regarding objects sitting on the table that would be difficult to acquire using one or more conventional cameras looking down at the table. In the future, sheet cameras may even be incorporated into clothing, making it easier for a wearable computer or a visually impaired individual to capture useful information in an inconspicuous manner.

Our objective is not to develop an end-to-end sheet camera system. Such an endeavor would be overly ambitious as it requires the use of various fabrication technologies that are each still in the research stage. Instead, our goal is to investigate the design of the optics needed to project images onto a flexible sheet with a regular grid of photosensitive detectors. At first glance one might imagine that a simple lens array aligned with a flexible detector array would suffice; its field of view (FOV) can be varied by simply bending it. What is perhaps less apparent is the fact that, in a curved state, the FOV can end up being severely under-sampled.

Consider the scenarios illustrated in Figure 2. When the sheet is perfectly flat, as in (a), all the sensing elements point in the same direction and, beyond a certain distance z_e, their fields of view are guaranteed to overlap. Now consider the case shown in (b), where the sheet is curved. Since the same number of sensing elements is used to sample a wider FOV, for some curvature of the sheet, the FOVs of adjacent elements will never overlap. In this setting, an object would be under-sampled irrespective of its depth. This under-sampling leads to a captured image that is not band-limited. Thus, the Nyquist sampling criterion is violated and the image will suffer from aliasing artifacts when reconstructed. An even more severe case is shown in (c), where the sheet has a sharp bend. At and around the bend, the captured image will have severe aliasing artifacts. It is important to note that these artifacts cannot be removed via post-processing since scene information is lost during image formation.

One way to avoid aliasing in cases like Figure 2 (b) and (c) is by ensuring that each lens in the array has a fixed but large field of view (FOV) that leaves no gaps between the FOVs of adjacent lens even when the array is curved. However, this approach will result in the lens array capturing highly blurred images when it is flat. Thus, with fixed FOV lenses, the image suffers from either alaising artifacts or excessive blurring no matter what FOV is choosen.

To avoid aliasing and blurring over all curvatures, we propose the design of a *deformable lens array*. We show that, if designed carefully, the deformable lenses of the array will change shape (and hence focal length) under bending forces in a way that mitigates aliasing and blurring. A remarkable feature of our design is that the lens array can achieve aliasing compensation without the use of any per-pixel actuation or control.

After summarizing related work, we describe the principle of passive optical adaptation. We present the desired adaptation curve which describes how the field of view of a lens must vary with local curvature to avoid aliasing. Next, we show how the geometry and material of the lens array can be chosen to achieve the desired adaptation curve. We use finite element analysis to simulate the deformation of our lens array and simulate images captured by it. These simulations demonstrate the anti-aliasing property of the lens array. Finally, we fabricate a lens array using silicone and attach it to an aperture array to emulate a sheet camera. We show image sequences of various scenes captured by flexing the sheet camera. We conclude the paper with a discussion on future work.

2. Related Work

To our knowledge, ours is the first attempt at developing a deformable lens array with intrinsic optical adaptation for anti-aliasing. Here, we describe several related works.

Two popular technologies used to actively control the shapes of deformable lenses are electrowetting [16, 23] and the use of electroactive polymers [14]. Another approach is to use fluid chambers with controlled pressure encased by flexible membranes [4, 5, 6]. There has also been previous work on the fabrication of flexible lens arrays for use in bendable displays. These include the use of polydimethylsiloxane (PDMS) droplets [24] and polymer-based lens arrays where focal length can be controlled using the polarization of incident light [17, 18]. Stretchable lens arrays have also been developed for low-cost solar energy concentration on spacecrafts [13].

In the context of imaging, there are two previous works that address the problem of capturing flexible fields of view.

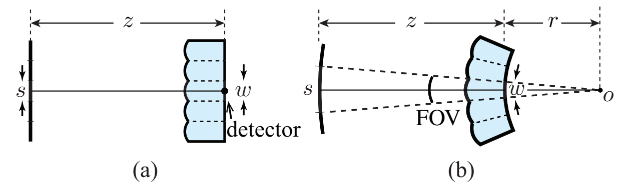

Figure 3. The lens array of the sheet camera in (a) planar and (b) curved states.

The first uses a conventional camera to image the world via a flexible mirror [10]. The second uses a flexible camera array where the captured images are stitched together to create a collage of the scene [11]. While the latter has a similar goal to ours - adjusting field of view using a flexible sheet - it differs in terms of the form factor and the geometric structure of the captured image. Our approach is geared towards the creation of imaging systems that are ultra-thin (like cloth and paper), a feature that is difficult to achieve using a collection of discrete cameras. Furthermore, while our sheet cameras capture contiguous fields of view, camera arrays produce images that are piece-wise perspective.

Recently, several lensless and thin imaging systems have been proposed. Koppelhuber et al. [8, 9] have developed a flexible image sensor using a transparent luminescent film. Abouraddy et al. [1] have developed a fiber that can be weaved to form a flexible image sensor that can measure the irradiance incident upon each point on it. Sorin et al. [21] use a similar approach to measure the direction and wavelength of incident light. Stork et al. [22] use a phase grating and a traditional CMOS sensor to capture a coded image that is processed to obtain a scene image. Finally, Asif et al. [2] have developed a flat imaging device by placing a coded aperture directly against a traditional image sensor. In our work, we are interested in the design of an optical system than can form a high-quality image on a flexible image sensor. Such an optical system can be used in conjunction with any flexible sensor such as the one developed by Kim et al. [7].

3. Lens Array with Passive Optical Adaptation

We first describe the property of a flexible lens array that is needed for it to exhibit passive optical adaptation. We model our array as a grid of identical plano-convex lenses, as shown in Figure 3(a). We refer to the convex side of each lens as the *front surface* and the planar side as the *base surface*. The detector grid of the sheet camera is attached to the base surface. For now, we assume the detector associated with each lens to be a single point.

The back surface of the sheet camera is assumed to be a deformable, developable surface, possibly with spatially varying curvatures and principal directions. Locally, any developable surface can be approximated as a cylinder with one of the principal curvatures equal to zero. Therefore, despite the fact that the sheet camera can be deformed in complex ways, the analysis of the mechanical and optical properties of any lens in the array can be done by assuming the deformation to be cylindrical.

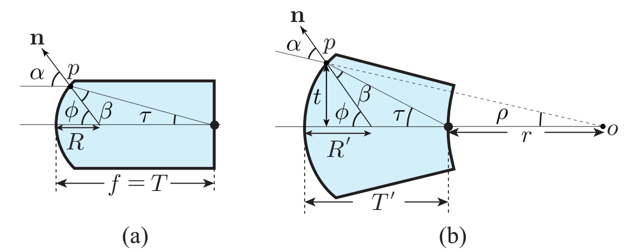

Figure 4. Lenses with the desired optical adaptation property in (a) the undeformed case and (b) the deformed case.

As shown in Figure 3, a single lens projects rays of light from a scene segment of size s at distance z onto its detector. We define the field of view (FOV) of the lens as the angle subtended by the segment s from the center of curvature o of the base surface. While for the flat array in Figure 3(a) the FOV is zero (the center of curvature is at infinity), for the deformed array in Figure 3(b) it is:

$$\text{FOV} = \frac{s}{z + 1/\kappa} = \frac{s\kappa}{z\kappa + 1}. \tag{1}$$

Irrespective of the shape of the lens array, to avoid aliasing, adjacent lenses should image adjacent segments in the scene without a gap between them. Furthermore, to avoid blurring in the captured image, the adjacent imaged segments should not overlap. For these conditions to be satisfied, the FOV must equal the angle subtended by the lens pitch w from the center of curvature o of the base surface:

$$\text{FOV}_{des} = w\kappa. \tag{2}$$

In short, irrespective of the shape of the sheet camera, the desired FOV of each lens is simply the product of the lens pitch w and the local curvature κ of the base surface.

4. Adaptation in Terms of Focal Length

We now relate the above expression for FOV adaptation to the focal length of the lens. This relationship is essential for understanding how each lens *should* deform in order to avoid aliasing and blurring in the captured image.

Whether the lens is undeformed (Figure 4(a)) or deformed (Figure 4(b)), any ray of light incident upon its front surface traveling towards the center of curvature o of the base surface, should be refracted by the lens towards the detector. Note that in the undeformed case the incident ray must be parallel to the lens's optical axis as the center of curvature is at infinity.

In the undeformed case, the focal length f of the lens should equal the thickness T, measured from the apex of

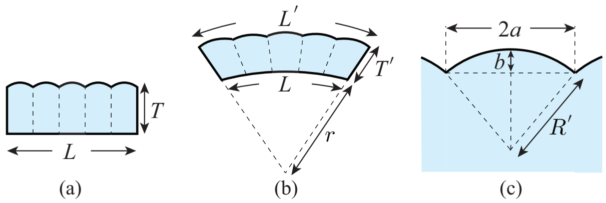

Figure 5. Ideal, incompressible deformation of a flexible lens array. (a) Undeformed array. (b) Deformed array. (c) Geometric parameters of lens deformation.

the lens to the base surface. However, this does not hold true when the lens is deformed. Hence, we derive an expression for focal length in terms of the radius R of the front surface, which is valid when the lens is undeformed and deformed.

Consider the undeformed case shown in Figure 4(a). From Snell's law, we have $\sin\alpha = \eta \sin\beta$, where α, β and η are the incident angle, refraction angle and the refractive index of the lens, respectively. We assume that in our setting the angles α and β are small and hence $\sin\alpha \approx \alpha$ and $\sin\beta \approx \beta$. As a result, $\alpha \approx \eta\beta$. Likewise, we have $f\,\tau \approx R\,\phi$, where τ is the angle between the optical axis and the refracted ray, and ϕ is the angle between the optical axis and the normal $\mathbf{n}$ of the front surface at the point of refraction p. Because the ray incident is parallel to the optical axis, we have $\alpha = \phi$. This gives us $\tau = \phi - \beta = \alpha - \alpha/\eta$. From the above relations, we get:

$$\frac{1}{f} \approx \frac{1}{R} \cdot \left(1 - \frac{1}{\eta}\right). \tag{3}$$

Next, we determine how the focal length should vary with the curvature $\kappa = 1/r$ of the base surface. We first start with the desired relationship between the thickness T' and the radius R' when the array is deformed. In Appendix A, we show this relationship to be:

$$\frac{1}{R'}\left(1 - \frac{1}{\eta}\right) \approx \frac{1}{T'} - \frac{1}{\eta}\frac{\kappa}{1+\kappa T'}. \tag{4}$$

The above relation is what we need to achieve the desired optical adaptation. From (3) and (4), we get an expression for the desired focal length of the lens under any deformation as:

$$\frac{1}{f_{des}} \approx \frac{1}{T'} - \frac{1}{\eta}\frac{\kappa}{1+\kappa T'}. \tag{5}$$

5. Deformation in Ideal Incompressible Case

We now assume the deformation of our lens array to be ideal (uniform over the array) and incompressible (volume preserving). With this assumption, we can determine how the thickness T' varies with curvature κ. We can then substitute for T' in (5) to obtain an expression for focal length adaptation that only depends on the initial shape of the lens and the curvature due to deformation.

As shown in Figure 5, we assume the base of the deformed array is a cylinder with curvature $\kappa = 1/r$, such that the base width L of the array remains unchanged and its side faces remain normal to the surface of the cylinder.

We first estimate the thickness T' and the radius R' of the front surface of a single lens of the deformed array, noting that all lenses are subject to the same deformation. From Figure 5(b), we can estimate the outer arc length L' of the entire array as:

$$L' = L \cdot (1 + \kappa T'). \tag{6}$$

Since the incompressibility condition requires that the volume of the array remain constant, we have $T\,L = T'\,(L + L')/2$, where T is the thickness of the lens when undeformed. Substituting in (6) and solving for T', we get:

$$\kappa T' = \sqrt{1 + 2\kappa T} - 1. \tag{7}$$

Now that we have estimated the thickness of a deformed lens, we get the final expression for the desired focal length f_{des} by substituting (7) into (5):

$$\frac{f_{des}}{T} = \frac{2\eta\sqrt{1+2\kappa T}}{\eta(1 + 2\kappa T + \sqrt{1+2\kappa T}) - 2\kappa T}. \tag{8}$$

Here, we have normalized the focal length f_{des} by the undeformed thickness T to make both sides of the equation dimensionless. This normalized focal length is scale invariant: the thickness and the desired focal length increase linearly with the scale of the array.

The above expression tells us how we would like the lens to adapt to deformation. In Appendix B, for comparison, we have derived the actual focal length of the lens under deformation:

$$\frac{f_{act}}{T} = \frac{(1+2\kappa T)(1+\sqrt{1+2\kappa T})a^2}{2(a^2+b^2)} + \frac{(\sqrt{1+2\kappa T}-1)b^2}{\kappa T(a^2+b^2)}. \tag{9}$$

Using this expression for the actual focal length of the deformed lens array, we can determine the maximum field of view FOV_{max} (bounded by the two extreme rays incident at the edges of the lens) as a function of the *normalized curvature* κT of the base surface. For the refractive index η we use 1.41, which is the index of the silicone rubber we used (Section 8). The maximum field of view FOV_{max} is shown (dotted blue plot) in Figure 6, and can be compared with the desired field of view FOV_{des} (black plot). These plots suggest that the adaptation of the actual lens is stronger than the desired adaptation. It must be noted, however, that FOV_{max} is determined using the limiting rays and the actual field of view obtained in practice is a

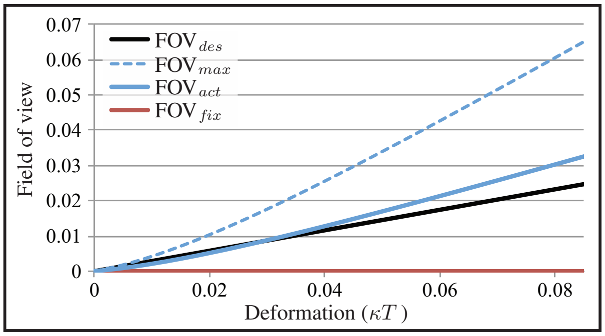

Figure 6. The desired field of view FOV$_{des}$, the maximum field of view FOV$_{max}$, the actual field of view FOV$_{act}$ and the fixed field of view FOV$_{fix}$, plotted as a function of the normalized curvature κT of the lens array. See Section 5 for details.

truncated version of FOV_{max}, where the truncation results from a physical aperture of finite thickness between the detector and lens. Such an aperture is also useful in ensuring that each detector only receives light from the lens above it and not adjacent ones. If we use an aperture that limits the maximum field of view by 50%, we get the actual field of view FOV_{act} (solid blue plot), which is very close in adaptation to the desired field of view FOV_{des}. If the lens array were made of a chain of rigid lenses (with fixed focal length), the array would not be able to optically adapt to curvature (red plot).

A sheet camera with a thickness T of 20mm, under the maximum deformation of $\kappa T = 0.085$ used in Figure 6, has a cylindrical base surface of radius 23.5cm. If the width of this camera is 74cm, the entire lens array will have a field of view of 180°. This design can be scaled up or down. For example, a sheet camera with a thickness of 2mm and a width of 7.4cm (the size of a credit card) can be deformed into a half-cylinder of radius 2.35cm to capture a 180° field of view. These examples suggest that sheet cameras can be deformed to capture aliasing-free images of very wide fields of view. It is also worth noting that the resolution of the camera can be increased by simply reducing the lens array pitch w without changing the thickness T and the radius R.

6. Choosing the Right Material

We have seen that if the lens array is made of an incompressible material, it will exhibit the type of adaptation we need to achieve optical anti-aliasing. It is known in continuum mechanics [20] that an elastic material is more or less incompressible if its Poisson's ratio is close to 0.5. Fortunately for us, there are several transparent elastic polymers that have Poisson's ratios in the range 0.48 to 0.49 [12].

Another consideration while choosing the material is its hardness, which is often measured on the Shore A scale [15]. The optically clear elastomers that are commercially available and suitable for our application have Shore A hardness values between 5 (soft) and 90 (hard). It is interesting to note that, regardless of the hardness of the material, its deformation properties are nearly constant as long as the Poisson's ratio is within the incompressible range.

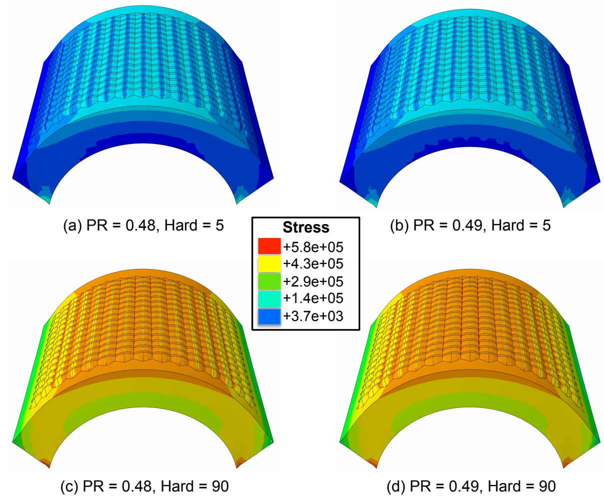

Figure 7. Abaqus simulations of a deformed lens array based on our design and made of materials with different Poisson's ratio and hardness values.

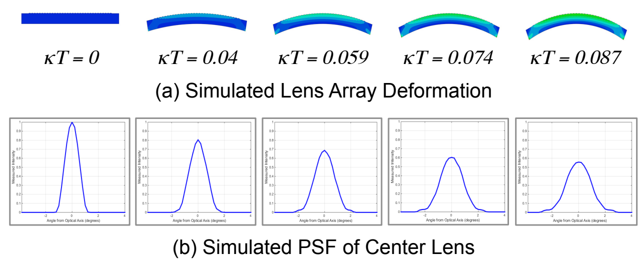

Figure 8. Object-side PSF of the center lens of the adaptive array for different array curvatures.

In Figure 7 we show four deformed lens arrays simulated using the finite element analysis package Abaqus [3]. We used Poisson's ratio values of 0.48 and 0.49 and Shore A hardness values of 5 and 90, which represent the limits of the ranges mentioned above. The color map is used to convey the mechanical stress within the array, where stress increases from blue to red. As expected, the stresses are higher in the harder materials. However, the four arrays are virtually identical in shape. The prototype lens we have fabricated (Section 8) uses a silicone rubber with a Poisson's ratio of 0.49, a Shore A hardness of 5 and a refractive index of 1.41. We chose a low hardness as it is easier to flex.

7. Verification of Optical Anti-Aliasing

To verify the efficacy of our deformable lens array, we compare its optical performance to that of a non-adaptive array, which consists of a grid of identical rigid lenses with equal and fixed focal length. For the geometry of the de-

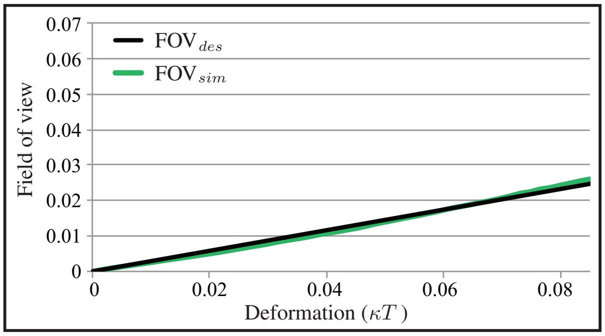

Figure 9. The field of view adaptation FOV_{sim} of the simulated deformable lens array is very close to the desired adaptation FOV_{des}.

formable array we used the Abaqus model in Figure 7(b), which has the following parameters: pitch $w = 7$mm, radius $R = 7.5$mm and thickness $T = 23$mm. Figure 8(a) shows the lens array under various deformations. We assume that the array was attached to an aperture sheet of thickness 2mm with a grid of apertures of diameter 0.5mm. The aperture parameters were chosen to achieve a field of view adaptation that is close to the desired one. For each curvature, we used the simulated shape of the center lens of the array to ray-trace its object-side point spread function (PSF). The resulting PSFs are shown in Figure 8(b). As expected, they get wider with the curvature of the array.

As in Section 5, instead of using the limiting rays to define the field of view, we can use the angle that contains a percentage of the energy within the PSF. If we choose this to be 85%, we obtain the adaptation curve FOV_{sim} shown in Figure 9, which is very close to the desired adaptation FOV_{des}.

Figure 10 shows the model we used for the non-adaptive lens array, where the focal lengths (and hence the PSFs) of all the lenses are the same and remain unchanged when the array is flexed. In this case, the PSF is assumed to be the first one shown in Figure 8(b), which corresponds to the undeformed (flat) state. As shown in Figure 10, when the lens array is curved, there are gaps between the FOVs of adjacent lenses, the size of the gap increasing with the curvature of the array.

Using our models for the adaptive and non-adaptive lens arrays, we generated the aliasing results shown in Figure 11. At the top is shown the scene texture which is the sum of two sinusoids, one low and one high in frequency. Using the known optical properties (PSFs and sampling period) of the two arrays, we rendered images captured by the two systems. For each curvature (κT) of the arrays, we assumed that the scene surface is also curved with the same center of curvature as the array. Since the FOV of the sheet camera increases with curvature, we interpolated the captured images in the horizontal direction to obtained stretched im-

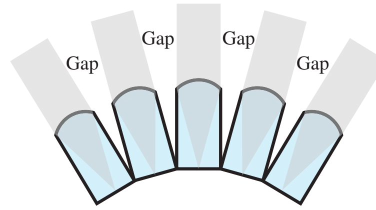

Figure 10. A non-adaptive lens array, where all the lenses are rigid with fixed and equal focal length. In this case, when the sheet camera is curved to be convex, there are gaps between the FOVs of adjacent lenses. Furthermore, since the lenses are rigid, the camera cannot be physically curved to be concave.

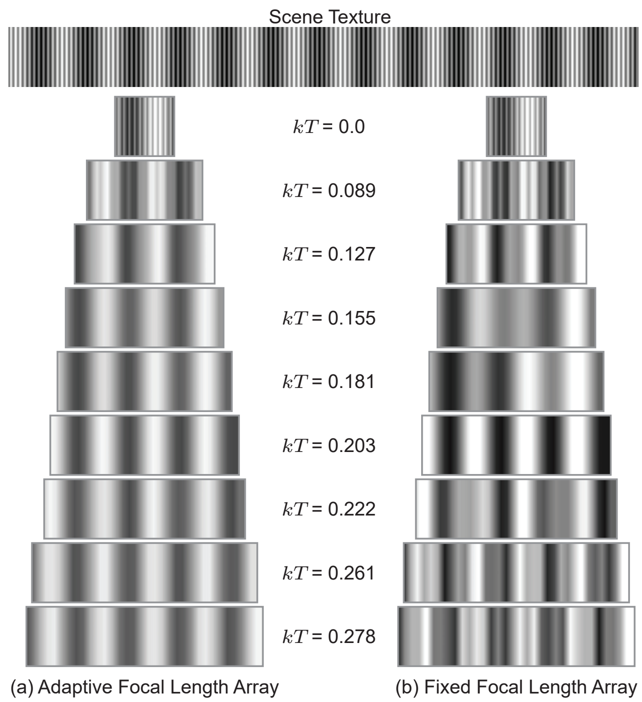

Figure 11. Images of a scene texture produced by the adaptive and non-adaptive arrays for increasing (top to bottom) deformations. While the adaptive array only blurs the scene texture for high curvatures, the non-adaptive array produces strong aliasing artifacts.

ages that depict the increasing horizontal FOV of the array. For the adaptive system, due to blurring, the high frequency sinusoid decreases in magnitude with curvature, while the low frequency sinusoid is faithfully reproduced over the entire range of deformations. In contrast, due to the narrow and fixed FOV of the lenses in the non-adaptive case, the scene texture is under-sampled for the higher curvatures which results in undesirable aliasing artifacts.

8. Fabrication of Flexible Lens Array

To test the concept of a sheet camera, we fabricated a 33x33 lens array using a liquid silicone rubber. The material properties and geometric parameters of the array are

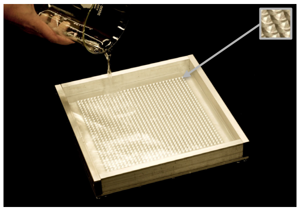
(a) Pouring Liquid Silicone Rubber in Mold

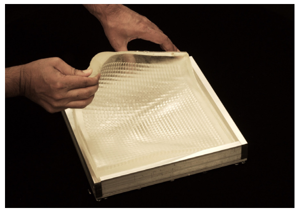
(b) Peeling Off Lens Array After Heat Curing

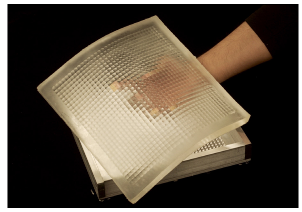
(c) Deformable Lens Array

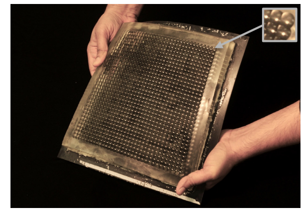
(d) Lens Array Attached to Aperture Sheet

Figure 12. Fabrication of the deformable lens array. (a) An aluminum mold for a 33x33 lens array was machined. A liquid silicone rubber solution was degassed to remove air bubbles and poured into the mold. (b) The solution was cured at 80° for 5 hours to solidify and the lens array was then peeled off. The array was glued to a flexible plastic sheet with a 2D aperture grid. A diffuser sheet is attached to bottom of the aperture sheet to form 33x33 images of the scene.

the same as those used in our simulations: Poisson's ratio = 0.49, Shore A hardness = 5, refractive index = 1.41, lens pitch $w = 7$mm, radius $R = 7.5$mm and thickness $T = 23$mm. We chose large values for the geometric parameters as it is easier to prototype a large scale system in the laboratory setting. By using a more advanced fabrication facility, however, the parameters can be significantly scaled down. As discussed in Section 5, it is possible to fabricate a lens array of the size of a credit card that has millions of lenses.

Figure 12 shows the process we used to fabricate our array. The mold, shown in Figure 12(a), was made of 6061 Aluminum by Contour Metrological and Manufacturing, Inc. with a maximum deviation from the prescribed shape of ± 0.05mm. The liquid silicone rubber we used is Momentive Silopren 7005. It consists of two components that are mixed in a beaker and placed in a vacuum chamber to remove air bubbles. Before pouring the liquid silicone into the mold, we cleaned the mold with soap and water, and then with acetone. Next, we sprayed the mold with a release agent to ensure that the lens array can be easily removed after curing. The liquid silicone was then poured into the mold, degassed to remove air bubbles, and cured in an oven at 80°C for 5 hours. Figure 12 (b) shows the cured lens being removed from the mold.

9. Prototype of Flexible Sheet Camera

In a complete implementation, the base surface of the lens array would be attached to a flexible 2D array of detectors. Since the development of such a detector array is a project unto itself, we have instead emulated the complete imaging system by glueing the lens array to a flexible plastic sheet of thickness 2mm with a rectangular grid of apertures of diameter 0.5mm. The pitch of the grid is 7mm to match the pitch of the lens array. Note that due to the finite thickness of the aperture sheet, each aperture limits the field of view of its lens to FOV_{sim}, as discussed in Section 7. An Optigrafix™ DFMM diffusing sheet is attached to the bottom of the aperture sheet to form a 33x33 optical image of the scene. The diffusing sheet is imaged by an digital camera to obtain a final image of the scene. As seen in Figure 12(d), the sheet camera can be flexed in various ways to control the field of view of the imaging system.

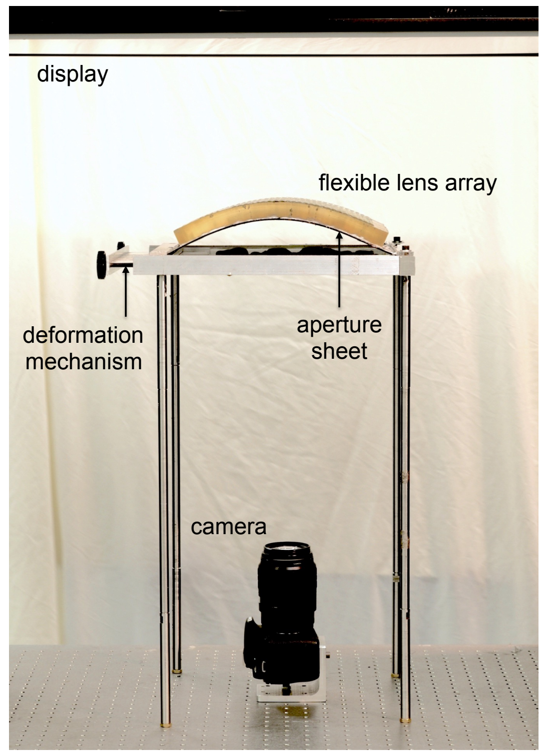

Figure 13. Experimental apparatus. The deformation of the flexible sheet camera is controlled using a vise-like mechanism. Images formed on the diffuser attached to the bottom of the sheet camera are captured using a digital camera and processed to produce 33x33 images of scenes shown on the display.

Figure 13 shows the experimental apparatus we have used to conduct our experiments. The deformation of the

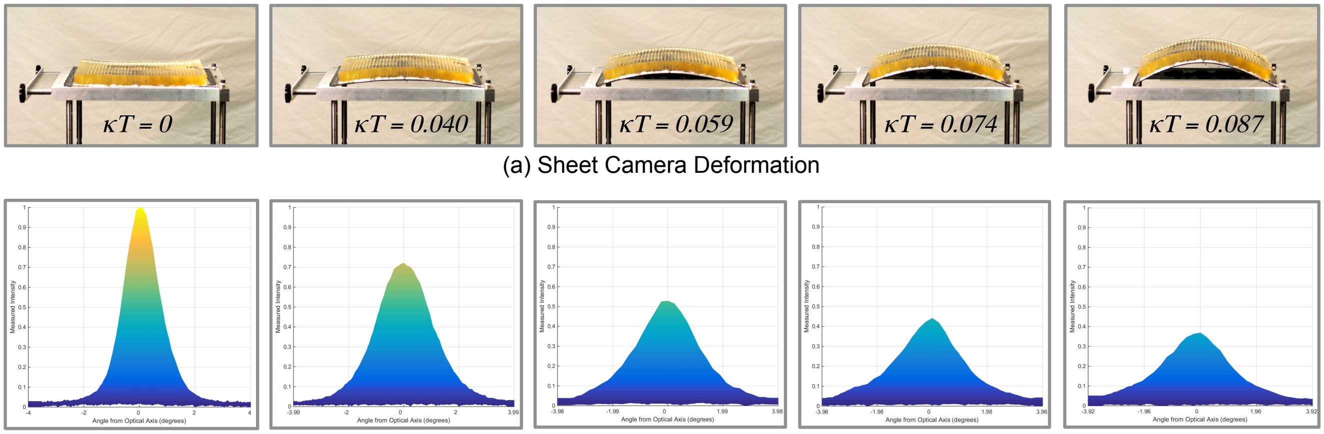

(a) Sheet Camera Deformation

(b) PSF of Center Lens

Figure 14. For each deformation of the lens array shown in (a), the measured object-side PSF of the center lens is shown in (b). Compare this adaptation of the PSF with the one shown in Figure 8.

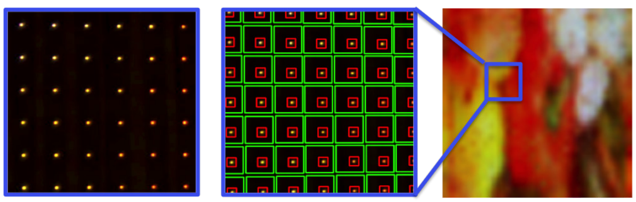

(a) (b) (c)

Figure 15. The process of converting an image of the diffuser sheet into an image of the scene. (a) A small part of an image of the diffuser taken with a high resolution digital camera. (b) Finding the locations and colors of the 33x33 spots in the image. (c) The final 264x264 image of the scene obtained by bicubic interpolation.

sheet camera is controlled using a vise-like mechanism - the parallel jaws of the vise push against two sides of the imaging sheet so that the distance between the jaws determines the curvature of the sheet. A Nikon D90 digital camera is used to capture images of the diffuser. These images have 33x33 dots that are detected and processed to construct the final image. Finally, to freely control the scenes shown to the imaging system, we have placed an LCD display above the flexible sheet.

10. Experimental Results

We have conducted several experiments to verify the ability of our sheet camera to optically adapt to deformations. First, we measured the object-side point spread function (PSF) of the center lens of the array as a function of local curvature. We varied the deformation of the lens array as shown in Figure 14(a). For each deformation we calculated the normalized local curvature κT of the center lens. For each setting, we raster scanned a small bright dot on the display and measured the brightness of the image on the diffuser produced by the center lens. Since this process involves a large number of high-resolution measurements, we used a video camera with a high-magnification lens in place of the SLR camera shown Figure 13. As seen in Figure 14(b), the measured PSF increases in width with curvature in accordance with our simulation results shown in Figure 8, demonstrating that the FOV of the lens does indeed increase with curvature to mitigate image aliasing.

In Figure 15 we show the image processing steps we use to convert a high resolution image of the sheet camera's diffuser into a 33x33 image of the scene. Figure 15(a) shows a small portion of an image captured by the digital camera. Each spot in this image is the image formed by a single lens of the array. First, the known shape of the sheet camera is used to estimate where the spots should show up in the digital image. These locations are represented by the green boxes shown in Figure 15(b). Next, within each green box, the centroid of the brightness distribution is used to locate the spot. Then, the average color within a smaller box around the centroid is computed to obtain the final color value for the corresponding lens. Using the principal ray of each lens, we project the corresponding color value onto a chosen surface (plane, cylinder, or sphere). These projected color values are then spatially interpolated, with the sampling frequency depending on the local curvature of the lens array, to obtain the final image. In the case of Figure 15(c), the color values obtained from 15(b) have been projected onto a plane and interpolated using a bicubic kernel to obtain a 264x264 image.

Figure 16 shows two image sequences captured using the prototype sheet camera. In the first column we show the deformation of the sheet, starting from the flat state where the angular field of view of the entire lens array is very small (the optical axes of all the lenses are parallel), to a highly curved state where the field of view of the lens array is $52°$ along the direction of deformation. The scenes shown to the sheet camera (second and third columns) are static and we see how the field of view increases in each case with sheet

Figure 16. Scenes captured by deforming the sheet camera. The first column shows the deformation of the sheet. The second column (colored dots scene) and third column (boy and horse scene) show images captured using the sheet camera and stretched using interpolation to account for the varying field of view of the deforming sheet. Due to the passive optical adaptation of the lens array, as the field of view of the sheet camera is increased (top to bottom), the captured images remain free of aliasing artifacts.

curvature. For any given sheet deformation, we know the directions of the optical axes of all the lenses of the array. This information is used to project the 264x264 captured image onto an plane of chosen distance from the sheet camera. This projection results in a stretching of each captured image based on the shape of the lens array. Due to the inherent optical adaptation of our design, the projected images, while blurred due to stretching, are free of aliasing effects. This is consistent with the anti-aliasing simulation results shown in Figure 11.

11. Future Work

We have presented the design of a lens array that enables a new class of flexible sheet cameras. We demonstrated via experiments that our lens array can be used to vary field of view while avoiding undesirable aliasing artifacts. The next step is to develop a high resolution version of the lens array and couple it with a large format image sensor of the type proposed in [8, 9]. A second approach is to develop an array of organic detectors that can be printed on a plastic sheet [19, 25].

Since the deformations used in our experiments were simple and controlled, we were able to easily determine the geometry of the sheet. In more advanced applications, such as wearable sheet cameras, the deformations would be complex and must be known so we can apply the appropriate geometric mappings to the captured images for either presentation to a human or for scene understanding by a machine. To this end, we plan to explore the idea of embedding a small number of stress sensors and/or accelerometers in the sheet and using the measurements from these sensors to compute the geometry of the sheet.

Finally, the sheet camera concept alleviates many issues faced by the conventional camera model. First, since the sheet is meant to be large enough to cover some meaningful area, it is inherently a large format camera. One way to think about such a camera is by imagining the millions of pixels of a phone camera to be distributed over a large area. In doing so, each sensing element of the sheet camera ends up being orders of magnitude larger than in the case of a conventional camera. This significant increase in pixel pitch has several advantages. First, the sensing area of each pixel can be made larger resulting in greater dynamic range and signal-to-noise ratio (SNR). Second, even after increasing the sensing area, we are left with plenty of real estate to use for circuits that would make the pixels more scene adaptive and intelligent.

Acknowledgments

This work was supported by ONR Grant No. N00014-14-1-0741 and ONR Grant No. N00014-16-1-2152. The authors are grateful to Behzad Kamgar-Parsi for his support and encouragement.

References

[1] A. F. Abouraddy, O. Shapira, M. Bayindir, J. Arnold, F. Sorin, D. S. Hinczewski, J. D. Joannopoulos, and Y. Fink. Large-scale Optic-field Measurements with Geometric Fibre Constructs. *Nature Materials*, 5(7):532–536, July 2006.

[2] M. S. Asif, A. Ayremlou, A. Sankaranarayanan, A. Veeraraghavan, and R. Baraniuk. FlatCam: Thin, Bare-Sensor Cameras using Coded Aperture and Computation. *arXiv:1509.00116v2*, 2016.

[3] Dassault Systemes. *Abaqus Unified FEA*. `http://www.3ds.com/products-services/simulia/products/abaqus/`, 2015.

[4] J. Fang, J. Chen, W. Wang, K. Varahramyan, R. A. Gunasekaran, and M. Agarwal. Wide-angle Variable Focal Length Lens System. *US Patent No. 7359124 B1*, April 2008.

[5] J. E. Floyd. Fluid Filled and Pressurized Lens with Flexible Optical Boundary Having Variable Focal Length. *US Patent No. 5684637 A*, November 1997.

[6] J. K. Guy. Flexible Lens. *US Patent No. 6542309 B2*, April 2003.

[7] D.-H. Kim, Y.-S. Kim, J. Wu, Z. Liu, J. Song, H.-S. Kim, Y. Y. Huang, K.-C. Hwang, and J. A. Rogers. Ultrathin Silicon Circuits With Strain-Isolation Layers and Mesh Layouts for High-Performance Electronics on Fabric, Vinyl, Leather, and Paper. *Advanced Materials*, 21(36):3703–3707, September 2009.

[8] A. Koppelhuber and O. Bimber. Towards a Transparent, Flexible, Scalable and Disposable Image Sensor Using Thin-film Luminescent Concentrators. *OSA Optics Express*, 21(4):4796–4810, February 2013.

[9] A. Koppelhuber and O. Bimber. LumiConSense: a Transparent, Flexible, and Scalable Thin-film Sensor. *IEEE Computer Graphics and Applications*, 34(5):98–102, September 2014.

[10] S. Kuthirummal and S. K. Nayar. Flexible Mirror Imaging. *ICCV Workshop on Omnidirectional Vision, Camera Networks and Non-classical Cameras (OMNIVIS)*, October 2007.

[11] Y. Nomura, L. Zhang, and S. K. Nayar. Scene Collages and Flexible Camera Arrays. *Proceedings of Eurographics Symposium on Rendering*, June 2007.

[12] G. P. O'Hara. Mechanical Properties of Silicone Rubber in a Closed Volume. Technical Report ARLCB-TR-83045, US Army Armament Research and Development Center, December 1983.

[13] M. J. O'Neill, A. J. McDanal, M. F. Piszczor, P. J. George, D. L. Edwards, H. W. Brandhorst, M. I. Eskenazi, M. M. Botke, and P. M. Jaster. The Stretched Lens Array (SLA): A Low-risk, Cost-effective Concentrator Array Offering Wing-level Performance of 180 W/kg and 300 W/m^2 at 300 VDC. *IEEE AESS Systems Magazine*, 18(1):3–9, January 2003.

[14] Optotune Switzerland AG. *Focus Tunable Lenses*. `http://www.optotune.com/products/focus-tunable-lenses`, 2015.

[15] H. J. Qi, K. Joyce, and M. C. Boyce. Durometer Hardness and the Stress-Strain Behavoir of Elastomeric Materi-

als. *ACS Rubber Chemistry and Technology*, 76(2):419–435, May 2003.

[16] C. Quilliet and B. Berge. Electrowetting: a Recent Outbreak. *Current Opinion in Colloid & Interface Science*, 6(1):34–39, February 2001.

[17] H. Ren, Y.-H. Fan, Y.-H. Lin, and S.-T. Wu. Tunable-focus Microlens Arrays Using Nanosized Polymer-dispersed Liquid Crystal Droplets. *Optics Communications*, 247(1-3):101–106, March 2005.

[18] H. Ren and S.-T. Wu. Polymer-based Flexible Microlens Arrays With Hermaphroditic Focusing Properties. *Applied Optics*, 44(36):7730–7734, December 2005.

[19] H. Saito, K. Hoshino, K. Matsumoto, and I. Shimoyama. Compound Eye Shaped Flexible Organic Image Sensor with a Tunable Visual Field. *Proceedings of the 18th IEEE International Conference on Micro Electro Mechanical Systems*, pages 96–99, February 2005.

[20] I. S. Sokolnikoff. *Mathematical Theory of Elasticity, 2nd ed.* McGraw-Hill, 1956.

[21] F. Sorin, O. Shapira, A. F. Abouraddy, M. Spencer, N. D. Orf, J. D. Joannopoulos, and Y. Fink. Exploiting Collective Effects of Multiple Optoelectronic Devices Integrated in a Single Fiber. *Nano Letters*, 9(7):2630–2635, June 2009.

[22] D. Stork and P. Gill. Optical, Mathematical, and Computational Foundations of Lensless Ultra-Miniature Diffraction Images and Sensors. *International Journal on Advances in Systems and Measurements*, 7(3 & 4):201–208, 2014.

[23] Varioptic. *Electrowetting*. `http://www.varioptic.com/technology/electrowetting/`, 2015.

[24] Y.-C. Wang, Y.-C. Tsai, and W.-P. Shih. Flexible PDMS Micro-lens Array with Programmable Focus Gradient Fabricated by Dielectrophoresis Force. *Microelectronic Engineering*, 88(8):2748–2750, August 2011.

[25] G. Yu, G. Srdanov, J. Wang, H. Wang, Y. Cao, and A. J. Heeger. Large Area, Full-color, Digital Image Sensors Made with Semiconducting Polymers. *Synthetic Metals*, 111-112:133–137, June 2000.

Appendix

A. Desired Relationship Between Lens Thickness and Lens Radius

As a lens experiences an increase in the local curvature, the lens radius will increase and the lens thickness will decrease. Both of these changes will affect the field of view of a lens. Thus, we seek to find the ideal relationship between change in radius and change in thickness of a single lens in relation to the local curvature. This relationship is ideal when the field of view of the lens is contiguous with its neighbors.

In the deformed case shown in Figure 17, we have:

$$\alpha = \phi - \rho \approx \frac{t}{R'} - \frac{t}{1/\kappa + T'}, \tag{10}$$

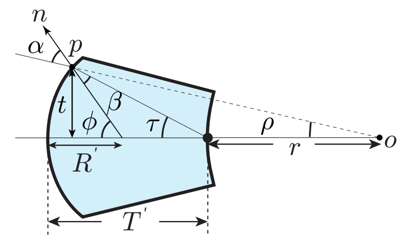

Figure 17. A lens with the desired optical adaptation property in the deformed case.

where t is the distance between the refraction point p and the optical axis, and T' is the thickness of the deformed lens. In addition, we have $\tau = \alpha - \beta + \rho = \alpha(1 - 1/\eta) + \rho$. Substituting (10), we get:

$$\tau \approx \frac{t}{R'}\left(1 - \frac{1}{\eta}\right) + \frac{1}{\eta}\frac{t}{1/\kappa + T'}. \tag{11}$$

Assuming $\tau \approx t/T'$, we obtain:

$$\frac{1}{R'}\left(1 - \frac{1}{\eta}\right) \approx \frac{1}{T'} - \frac{1}{\eta}\frac{\kappa}{1 + \kappa T'}. \tag{12}$$

B. Actual Focal Length as a Function of Normalized Curvature

To find the actual focal length, we must first understand how R' changes with local curvature. To estimate the radius R' of the deformed front surface, we simplify our system to a section of a circle. Given an arc with chord length $2a$ and chord height b, the radius of the front surface is $R' = (a^2 + b^2)/(2b)$. Initially, in the undeformed case, we have $a = w/2$, where w is the lens' width and $b = R - \sqrt{R^2 - a^2}$. In the deformed case, we approximate the deformed chord length $2a'$ and chord height b' as $a' \approx aL'/L$ and $b' \approx bT'/T$, respectively. L' can be found by substituting (7) into (6) to obtain $L' = L \cdot \sqrt{1 + 2\kappa T}$. From the above relations, we have:

$$\frac{R'}{R} = \frac{(L'/L)^2 a^2 + (T'/T)^2 b^2}{(T'/T)(a^2 + b^2)}. \tag{13}$$

For the initial radius R, we subsititute $\kappa = 0$ in (4) to get:

$$R = T \cdot \frac{\eta - 1}{\eta}. \tag{14}$$

From (3), (7), (13) and (14) we obtain the following expression for the actual focal length (15).

$$\frac{f_{act}}{T} = \frac{(1 + 2\kappa T)(1 + \sqrt{1 + 2\kappa T})a^2}{2(a^2 + b^2)} + \frac{(\sqrt{1 + 2\kappa T} - 1)b^2}{\kappa T(a^2 + b^2)}. \tag{15}$$